Journal of Hydroscience and Hydraulic Engineering
Vol. 30, No.1 May, 2012, 29-46

STUDY ON LOCAL SCOUR AND VARIATION OF BED COMPOSITION AROUND NON-SUBMERGED SPUR DYKE

By

Hideaki Mizutani

Graduate School of Civil and Earth Resources Engineering, Kyoto University, Katsura Nishi-ku, Kyoto, Japan

Hajime Nakagawa

River Disaster Prevention System, Research Center for Fluvial and Coastal Disasters,
Disaster Prevention Research Institute, Kyoto University, Yoko-oji Fushimi-ku, Kyoto, Japan

Kenji Kawaike

River Disaster Prevention System, Research Center for Fluvial and Coastal Disasters,
Disaster Prevention Research Institute, Kyoto University, Yoko-oji Fushimi-ku, Kyoto, Japan

Yasuyuki Baba

Field Research Section for Fluvial and Coastal Hazards, Research Center for Fluvial and Coastal Disasters,
Disaster Prevention Research Institute, Kyoto University, Shirahama Muro-gun, Wakayama, Japan

and

Hao Zhang

River Disaster Prevention System, Research Center for Fluvial and Coastal Disasters,
Disaster Prevention Research Institute, Kyoto University, Yoko-oji Fushimi-ku, Kyoto, Japan

SYNOPSIS

Several studies have been made on local bed scour by means of movable bed experiments. However, researches which have taken into account non-uniform sediment transport are still very limited, particularly in cases where spur dykes are involved. In this study, we carried out movable bed experiments around single impermeable spur-dyke under non-submerged conditions. Both uniform and non-uniform sediment beds with similar mean diameters were used and the changes of the bed configuration and bed surface composition were also considered. In addition, we used color sediment which was divided in three ranges of diameter with different colors in order to clarify the spatial differences of bed surface composition by using pictures and visual observation. Finally, we focused on

the relation between initial grain-size distribution and the final scour-hole depth and the influence of vortices around a spur dyke on bed surface composition.

INTRODUCTION

In recent years, concern about river environment has grown. In general, the purposes of building spur dyke are to protect channel banks and to improve navigation conditions. However, spur dykes are also considered as potential measures to enhance diversities of channel morphologies and riverine eco-systems. Recently, the investigation of the environmental implications and improvements by means of installing spur dykes has attracted much interest. For example, Shimizu et al. (1) and Fukudome et al. (2) have studied spur dykes based on actual rivers, and generated bed deposition-erosion to restore pool-riffle morphology.

Spur dykes are typical hydraulic structures and the investigation of flow structure and scour mechanism around spur dykes is very interesting and it is a vital research topic in the field of river engineering. Michiue and Hinokidani (3), Muneta and Shimizu (4) and Zhang et al. (5) measured the flow field around impermeable spur-dyke. Tominaga et al. (6) focused on three-dimensional flow structure around submerged spur-dyke and investigated by Particle Image Velocimetry (PIV) analysis. Many experimental studies of local scour around spur dyke have also been reported in various literatures. In order to estimate the maximum scour depth, many prediction formulae of equilibrium scour depth have been developed, e.g. Melville (7); Rahman and Muramoto (8); Nasrollahi et al. (9). Furthermore, since there are many design parameters (length, impermeable or permeable, alignment, angle with bank, and number of spur dykes), and there are also many combinations of them, so numerical models have been developed to improve its design. Numerical simulation is useful tool to determinate the appropriate design of a spur-dyke. Therefore, extensive research has been conducted into developing numerical models, e.g. Michiue and Hinokidani (3); Muneta and Shimizu (4); Nagata et al. (10); Zhang et al. (11). However, time have not passed so much since the numerical model can be used to reproduce flow field and bed variation with enough accuracy for use in prediction. In addition, there has been no study that has attempted to reproduce not only the bed topography but also bed composition around a spur dyke.

It is widely known that the composition of bed surface has a significant impact on the scour process and habitats of aquatic plants and animals. But researches that have focused on bed composition changes around spur dykes are still scarce because of the complexity of phenomenon and necessity of heavy work to obtain the results (Duan et al. (12); Zhang et al. (13)). Therefore, the influence of grain size distribution on bed variation and the spatial grain size variation around a spur dyke has not been clarified yet. Furthermore, we expected that accumulation of bed composition data can be useful for developing a numerical model, which is applicable for non-uniform sediment with good precision.

In this study, we have attempted to clarify the impact of grain size distribution on the bed topography and to clarify the spatial variation of surface bed composition around a spur dyke by means of experimental methods. To begin with, we conducted fundamental movable bed experiments by using uniform/non-uniform sediments bed with single impermeable spur-dyke under non-submerged condition and clear-water condition.

EXPERIMENTS AND METHODS

Experimental flume setup

A series of experiments were performed in a rectangular flume 8m long and 0.4m wide with a bed slope of 1/1000 at Ujigawa Open Laboratory, Disaster Prevention Research Institute, Kyoto University (Japan). A sediment recess 0.2m deep, 0.4m wide and 1.7m long, was made 4m downstream from the flume inlet as shown in Fig. 1. The flume had a re-circulating water supply system. A soft and permeable pad was set near the junction of inlet tank, which was installed to inhibit flow concentrations and to minimize the wavy surface. The experiments were carried out by means of an impermeable spur-dyke attached to the flume. The spur dyke was set perpendicular to the right side of the flume wall with a protruding length of 10cm and was kept non-submerged condition during the experiments. The hydraulic conditions before the installation of the spur dyke on flatbed are shown in Table 1. All the experiments were conducted under the same approach-flow conditions.

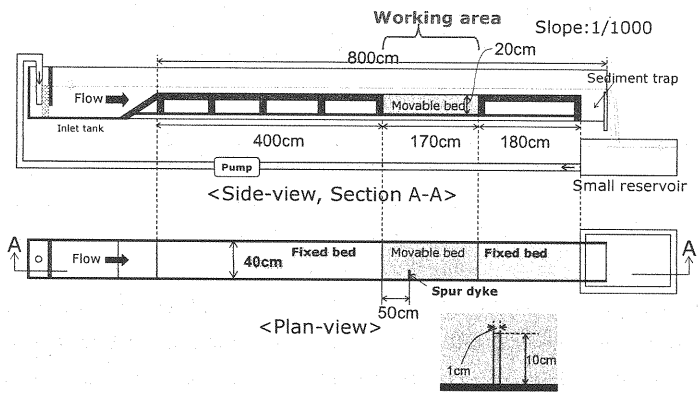

Fig. 1 Details of the experimental flume setup

Table 1 Hydraulic and spur dyke conditions

Flow discharge Q (l/s)	5.7
Channel slope I	1/1000
Channel width B (cm)	40.0
Flow depth h (cm)	5.0
Flow velocity U (cm/s)	28.5
Friction velocity U_* (cm/s)	1.98
Reynolds number Re	14,250
Froude number Fr	0.41
Spur length L (cm)	10.0
Spur thickness b (cm)	1.0

Two series of experiments were conducted, which consisted of 9 cases totally (Table 2). The first series was composed of 4 cases and tested the effects of mean grain size on the bed topography around the spur dyke using relatively uniform sediment particles (referred to as U-series hereafter). While the remaining 5 cases belonged to the second series which tested the impact of sediment size distribution on the bed topography and variation of the surface

sediment size distribution around the spur dyke using sediment mixtures of various size distribution (referred to as M-series hereafter).

Table 2 Experimental conditions for all cases

Case No.	Case name	D_{m0} (mm)	σ_g	U_*/U_{*c}
1	U1	0.31	1.36	1.18
2	U2(M0)	1.03	1.23	0.83
3	U3	1.70	1.18	0.62
4	U4	2.38	1.48	0.49
5	M1-WG1	0.86	2.36	0.91
6	M2-CS	1.01	2.55	0.85
7	M3-GG1	1.00	2.62	0.85
8	M4-WG2	1.01	3.62	0.84
9	M5-GG2	1.05	4.30	0.82

D_{m0}: Initial mean diameter
σ_g: Geometric standard deviation
U_*/U_{*c}: Critical friction-velocity ratio

The experiments were carried out with various bed conditions. Four cases of relatively uniform sediments and five cases of mixture sediments were prepared by mixing different sizes of sediments. The grain size distributions of sediment particles at the initial bed are shown in Fig. 2. In the U-series experiments, the mean grain sizes were 0.31, 1.03, 1.70 and 2.38mm from Case U1 to Case U4, respectively. Correspondingly, the shear velocity ratio U_*/U_{*c}, indicating the sediment particle mobility, were 1.18, 0.83, 0.62 and 0.49, respectively, where U_{*c} is the critical friction velocity for sediment entrainment. In the M-series experiments, the initial mean grain size D_{m0} of each case was made similar to that of Case U2, while the geometric standard deviation σ_g varied as shown in Table 2. In the cases of Mix-WG2, Mix-WG2 and Mix-CS bed sediments, the grain size distribution curves were relatively smooth and well graded as shown in Fig. 2. The Mix-GG1 and Mix-GG2 bed cases adopted gap-graded particles consisting mainly of two grain size: a coarse one and fine one. In order to understand the phenomenon more visually, color sands were utilized in Mix-CS experiments (Fig. 3). Relatively uniform sediment particles of black, blue and red colors were fully mixed for the preparation of the non-uniform sediment bed. The black particles had a grain size ranging from 1.40mm to 2.36mm, and the blue ones from 0.5mm to 1.40mm, and the red ones from 0.125mm to 0.5mm.

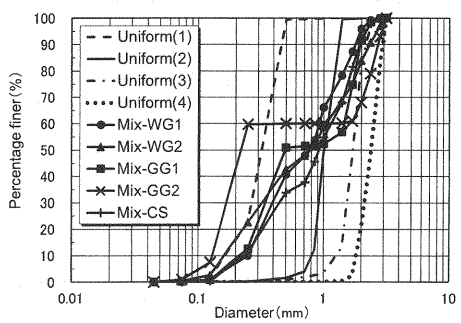

Fig. 2 Grain size distributions of sediment particles at initial bed

Table 3 Description of each bed conditions

Bed Name	Initial Bed condition for (Dm) and (σ_g)	Description of sediment mixtures
Uniform	(1) D_{m0}=0.31 , σ_g=1.36 (2) D_{m0}=1.03 , σ_g=1.13 (3) D_{m0}=1.70 , σ_g=1.18 (4) D_{m0}=2.38 , σ_g=1.48	Relatively uniform sediment.
Mix-GG1	D_{m0}=1.00 , σ_g=2.62	**Gap-graded** particles mainly consist of 2 grain size.
Mix-GG2	D_{m0}=1.05 , σ_g=4.30	**Gap-graded** particles mainly consist of 2 grain size.
Mix-WG1	D_{m0}=0.86 , σ_g=2.36	The size distribution curve is relatively smooth and sediment particles are relatively **Well-graded**.
Mix-WG2	D_{m0}=1.01 , σ_g=3.62	The size distribution curve is relatively smooth and sediment particles are relatively **Well-graded**.
Mix-CS	D_{m0}=1.01 , σ_g=2.55	The size distribution curve is relatively smooth and sediment particles are relatively **Well-graded**. (**Color sand**)

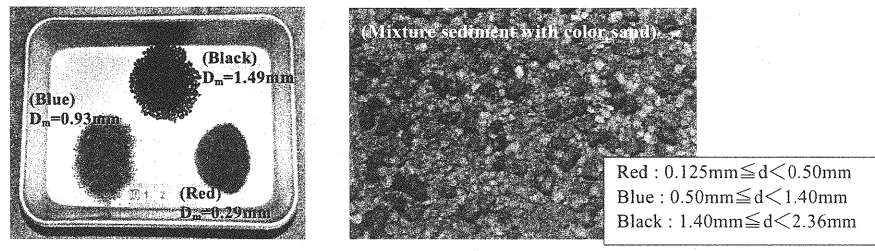

Fig. 3 Bed material for color-coded sediments

Experiment procedure

Before starting each experiment, the movable bed in the recess basin was leveled with a scraper blade mounted on a carriage riding on the rails over the model channel banks. Then, the flume was slowly filled with water from the downstream end of the flume. When the desired water depth was achieved by adjusting the height of the tailgate at end of the flume, the designated water supplied from the upstream end of the flume by using a pump system to start the experiments. Each experiment was run for 3 hours, which was long enough for the establishment of a quasi-equilibrium stage.

After the completion of each experiment, the flume was drained out and the bed configuration was measured with a high-resolution laser displacement meter (Model LK-500, Keyence, co., Ltd.). After that, sediment samples were taken carefully from the bed surface (about 2.8mm thick within 3cm in diameter) by using scoopula at several representative locations in the M-series experiments. The size distributions of the samples were analyzed with a nested column of sieves. Since bed scours and deposition patterns were similar at the quasi-equilibrium stage, the flow field was measured only for representative cases (i.e., Case U2). Before the measurements of the flow field, the deformed bed was fixed by using instant cement after the flume was completely drained out. Then, a constant water discharge was supplied from the upstream end of the flume. PVC (Polyvinyl chloride) tracers were distributed in the flume and videos were recorded for PIV (Particle image velocimetry) analysis of the surface velocity. Under the water surface, velocity fields in several specific longitudinal and transverse sections were measured with an EMV (Electromagnetic velocimeter, Model ACM250-A, JFE Alec Co., Ltd.). The frequency of flow measurement was 20Hz and the number of measuring was 750. The measured mean flow fields, which are shown in the next chapter, were averaged in this period. For the color sand case (i.e., M2-CS) a series of pictures was taken at regular intervals to capture the expanding process of the scour and sorting around the spur dyke with a DSLR camera (Nikon D5000).

RESULTS AND DISCUSSIONS

Scour-hole expansion

Local scour developed rapidly at the toe of the spur dyke in the first several minutes. Then, the scour-hole had been expanded due to the horse-shoe vortex, which was accelerated by down-flow in front of the spur dyke. Fig. 4 shows the process of scour-hole expansion for the upstream side of spur dyke. The lines in Fig. 4 indicate the time variation of scour-hole edge until 90 minutes. According to the figure, we found that the scour hole had been rapidly expanded concentrically from the spur dyke head at incipient stage. As time passed, the scour hole expanded slowly due to sliding of the edge part sediments toward the inner region as the degradation of the bottom bed around the spur dyke. In addition, the expansion speed of scour hole near the side wall was a somewhat faster than detached place from the spur dyke.

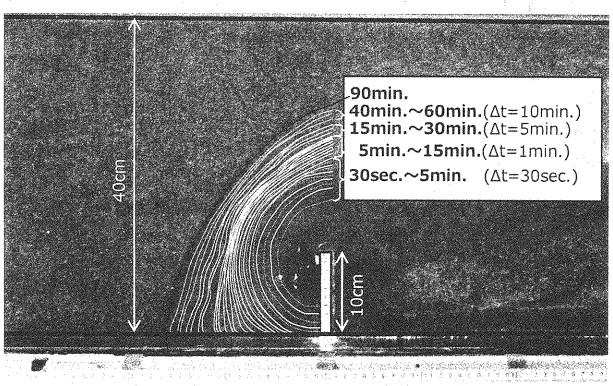

Fig. 4 Scour-hole expansion of the upstream part (Case 6)

Uniform sediment bed

The bed contour for each U-series experiment cases at the quasi-equilibrium stage are shown in Fig. 5. Each experiment was run for three hours, which was long enough for the establishment of a quasi-equilibrium stage. At this stage, sediment transport was slight and the variation of the bed topography was insignificant. It was evident that the bed topography around the spur dyke was characterized by a local scour near the toe of spur-dyke and a predominant deposition area downstream of the spur dyke. For clarity, a sketch of the dimensions of local scour is shown in Fig. 6 and several key parameters representing the bed topography features are listed in Table 4. In the analyses, the maximum scour depth was normalized with the flow depth and the spur dyke length.

In uniform sediment bed, the mean grain size played the most important role in scouring. Since the conditions of flow approach were kept the same for all experiments, the mean grain size was directly related to the particle mobility and hence the bed deformation. Figs. 5 (a) to (d) indicated that the scoured area reduced with each increase in the mean grain size. The values of a/L, b/L, c/L and d/L in Table 4 which express the dimension of the scour hole, gave more quantitative evidences. Besides the maximum scour depth decreased with the increase of the mean grain size as well (Table 4 and Fig. 7). The position of the deepest point located near the toe of the spur dyke in relatively coarse sediment bed (Case U4) and gradually shifted to the side of the flume when the bed materials became finer.

The slope of the scour hole in the downstream (θ_3) was much milder compared with that in the upstream and transverse slopes (θ_1, θ_2) in Table 4. The difference of scour-hole slope was due to the existence of predominant down-flow at downstream of the spur dyke toe, it will be discussed later. The down-flow caused conspicuous scouring there, and the scour-hole slope became milder than that in the upstream and transverse directions. In addition, if different cases were analyzed, the local slope generally became steeper when the bed materials became coarser (Table 4).

The mean grain size not only influences the bed degradation around the spur dyke but also the deposition at downstream of spur dyke. It was clear that the predominant deposition areas were located near the downstream of spur dyke in a coarser bed. The deposition areas usually moved away from the spur dyke as the bed materials became finer. The mobility of sediment particles can help explain the differences in the features of deposition: coarse particles were hard to move but easy to deposit. Case U1 required special attention since it was conducted under live-bed scour condition. Development of bed forms were observed in Case U1, which had a particle mobility parameter U_*/U_{*c} over unity. The superimposition of the bed forms on the deposition caused by the existence of the spur dyke might have some influence.

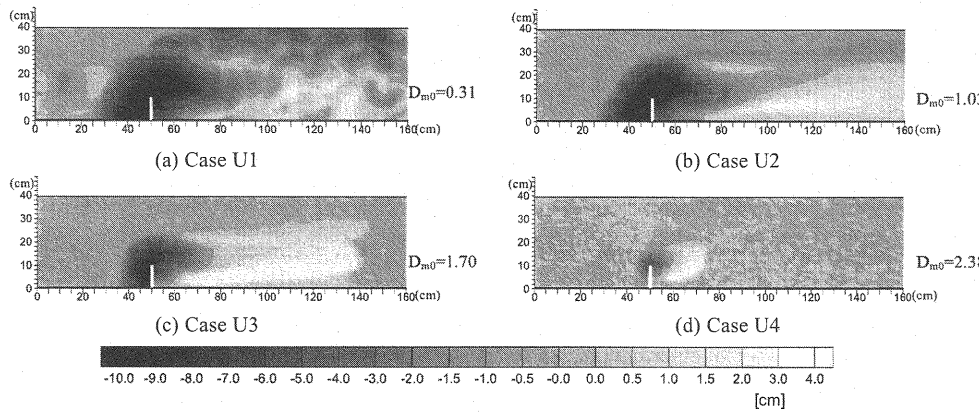

Fig. 5 Bed contour at the quasi-equilibrium stage for uniform sediment bed

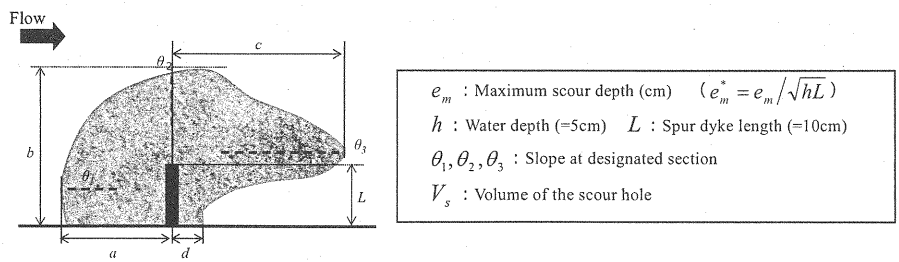

Fig. 6 Sketch of scour-hole dimensions and several key parameters

Table 4 Bed topography features for uniform sediment bed

Case No.	1	2	3	4
Case Name	U1	U2(M0)	U3	U4
a/L	2.4	2.1	1.4	0.6
b/L	4.0	2.9	2.3	1.6
c/L	3.9	4.0	2.1	0.9
d/L	1.4	1.4	0.0	0.0
θ_1(°)	27	27	34	39
θ_2(°)	29	31	33	39
θ_3(°)	14	12	17	25
e_m(cm)	12.6	11.7	9.25	5.5
e_m*	1.79	1.66	1.31	0.78
V_s(cm^3)	7262	5978	2378	268

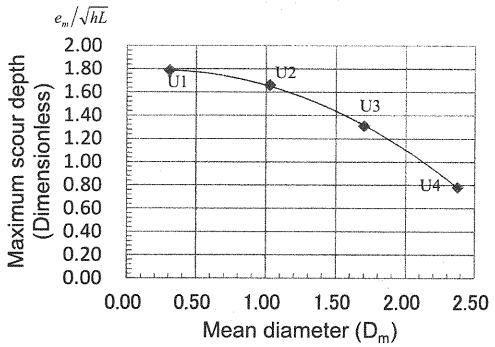

Fig. 7 Relation between maximum scour depth and mean diameter

Non-uniform sediment bed

Figure 8 indicates that the sediment heterogeneity did not exert impact on the general scour-deposition spatial pattern in the bed topography around the spur dyke. In Fig. 9, it was found that the maximum scour depth monotonically decreased with the increase of the geometric standard deviation σ_g, and the relationship between them was almost linear. The reason for the decrease of scour depth in non-uniform sediment was the formation of an armor layer at the bottom of the scour hole. During the scour process, relatively fine sediments were picked up and the bed was gradually coarsened, preventing the bed from further degradation. Since the geometric standard deviation σ_g implied coarse sediment fractions in non-uniform sediment, such a relationship exists as shown in Fig. 9. M5 bed sediment was gap-graded consisting of two grain sizes, which was the largest difference in grain size under the condition of similar mean grain size in this study. Although M5 bed included a large amount of fine sediment compared with other non-uniform bed cases, the maximum scour depth was the smallest in M-series experiments, because M5 bed also included a large amount of coarse sediment. These results indicated that the initial rate of coarse sediment, which can form an armor layer, was important in reducing the maximum scour depth in non-uniform sediment bed.

The difference of grain size distribution also influences the deposition area in a non-uniform sediment bed. With the increase of σ_g, the location of deposition area shifts nearer to the spur dyke. Since parameter of σ_g implied a larger portion of coarse fractions in sediment mixtures, the trend of deposition area can be explained.

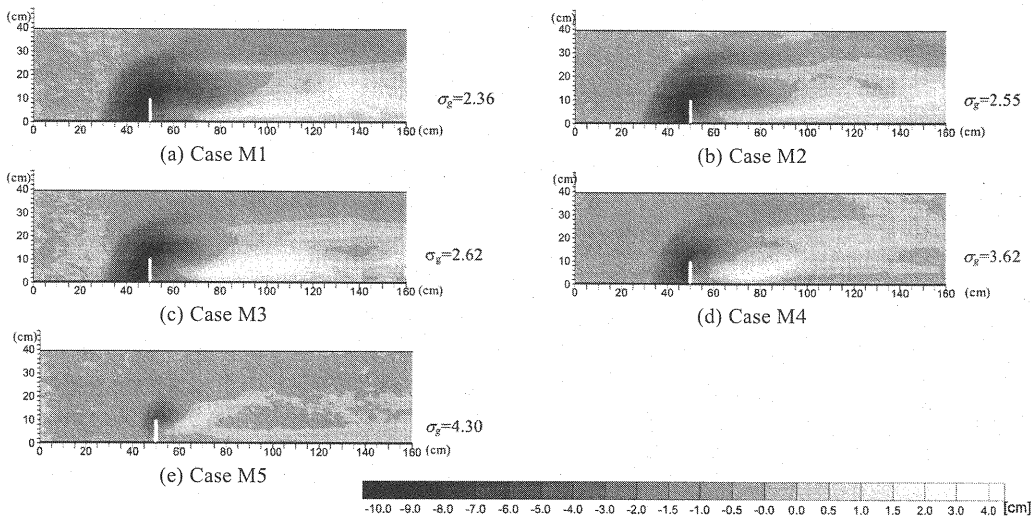

Fig. 8 Bed contour at the quasi-equilibrium stage for non-uniform sediment bed

Table 5 Bed topography features for non-uniform sediment bed

Case No.	2	5	6	7	8	9
Case Name	U2(M0)	M1	M2	M3	M4	M5
a/L	2.1	2.1	2.1	1.9	1.6	0.7
b/L	2.9	3.0	3.0	2.9	2.2	2.0
c/L	4.0	3.7	3.7	2.3	1.6	1.0
d/L	1.4	0.9	1.0	0.4	0.0	0.0
θ_1(°)	27	22	20	26	21	34
θ_2(°)	31	25	24	26	21	27
θ_3(°)	12	10	12	16	17	16
e_m(cm)	11.7	9.6	9.3	9.2	7.5	5.3
e_m*	1.66	1.36	1.32	1.31	1.06	0.75
V_s(cm^3)	5978	4532	4026	3210	1964	353

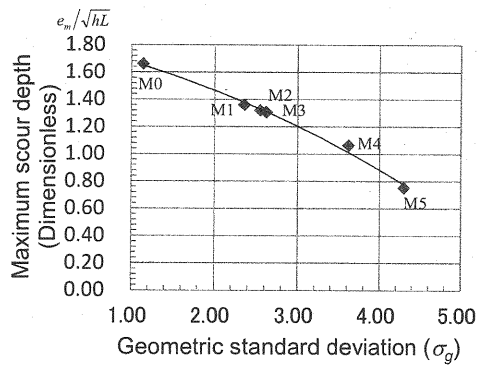

Fig. 9 Relation between maximum scour depth and geometric standard deviation

Flow structure around a spur dyke

Several studies have been made on the flow structure around spur dyke. Experimental studies by Michiue and Hinokidani (3), Zhang et al (5) have focused on the flow structure around non-submerged spur dyke on the scoured bed. The data of flow structure around the spur dyke on scoured bed measured by previous researchers are not sufficient, especially to account for the mechanism of sediment sorting around the spur dyke. In this study, we measured the detailed three-dimensional flow field to clarify the mechanism of sediment sorting around spur dyke. Since bed scour and deposition patterns in all experiments were similar at the quasi-equilibrium stage, flow field was measured only for one case in this study. We could predict that the flow structure would be generally similar for all cases.

Figure 10 shows time-averaged velocity and stream line on the water surface, which was obtained by the PIV analysis. In the non-submerged spur dyke condition, the surface flow was reduced in front of the spur dyke and at the downstream region of the spur dyke. The surface flow structure behind the spur dyke appeared as a fan-shaped structure owing to the upwelling from wake vortex system.

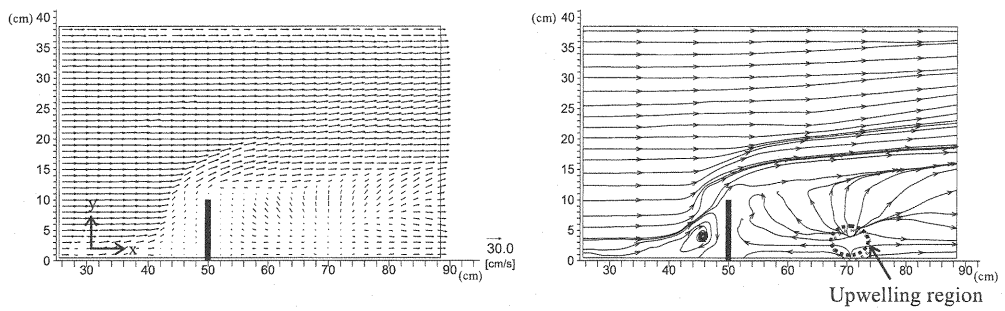

Fig. 10 Velocity vector (*u, v*) and stream line at the surface flow under scoured bed

In order to clarify the detailed three-dimensional flow structure around spur dyke, we measured the velocity fields with EMV in several representative transverse and longitudinal sections as shown in Fig. 11. The longitudinal measurement sections are shown in Fig. 12, and detailed longitudinal sections in upstream scour hole are shown in Fig. 13, while the transverse sections are shown in Fig. 14.

In front of spur dyke region, the remarkable down-flow, which occurred due to pressure gradient, was measured as shown in Fig. 12 and Fig. 13. The down-flow not only occurred in front of spur dyke but also at downstream of the spur dyke toe in shown Fig. 12 (c). Figure 12(c) shows the velocity vector at the (y=15cm) longitudinal section, which was located near the spur dyke toe and deep scoured region extending to downstream. The region of longitudinal section equal to y=15cm was located in a high-concentration of flow due to the flow deflection effect as shown in Fig. 10. The vertical velocity of down-flow had the value of approximately 40 percent of the approach flow velocity in this experiment. The detailed flow measurement in the scour-hole shows that the horse-shoe vortex system consists of two vortices structure in same direction of rotation near the sidewall, and these two vortex structures disappeared near the spur dyke toe (in Fig. 13). The horse-shoe vortex was located in the scour hole and the vortex axis bent along the scour-hole edge. The velocity of horse-shoe vortex gradually became weak as it moved away from the spur dyke in downstream direction. Behind the spur dyke, another vortex appeared referred to as a wake vortex, and whose rotation was the reverse of the horse-shoe vortex. There was remarkable down-flow

between the horse-shoe vortex and the wake vortex, and the down-flow was the driving force on two vortices. Furthermore, the third vortex was measured near the sidewall as shown Fig. 14 (g), (h). The third vortex resulted from the wake vortex and bed shape behind the spur dyke. The third vortex caused the deposition area which moved slightly to the inner region from the sidewall.

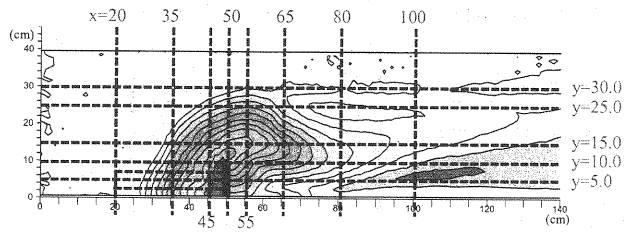

Fig. 11 Measurement sections of flow velocity with EMV

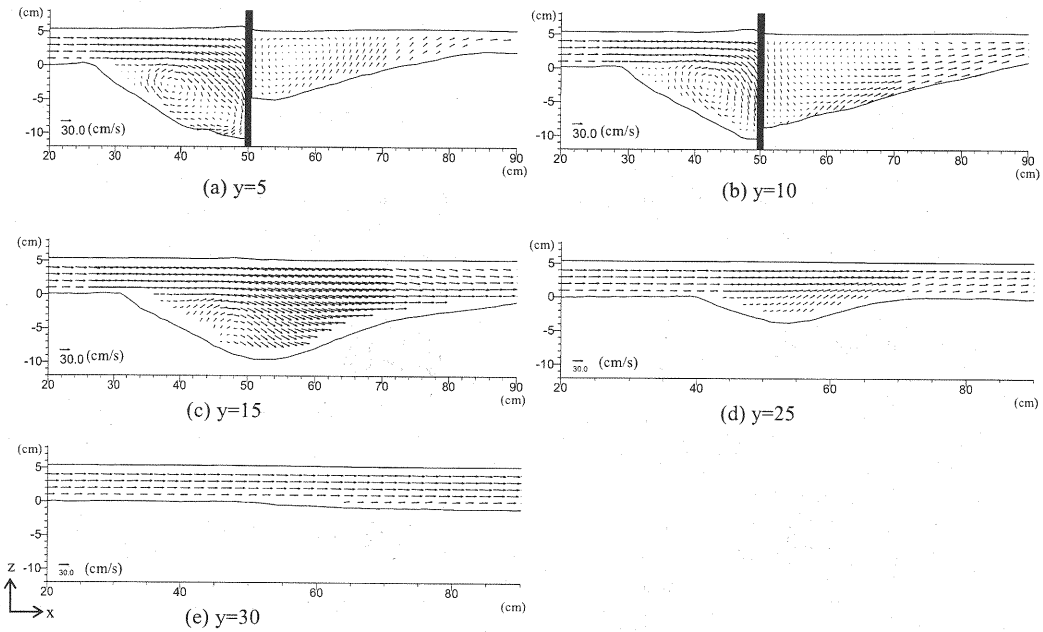

Fig. 12 Velocity vector (u, w) at the longitudinal sections

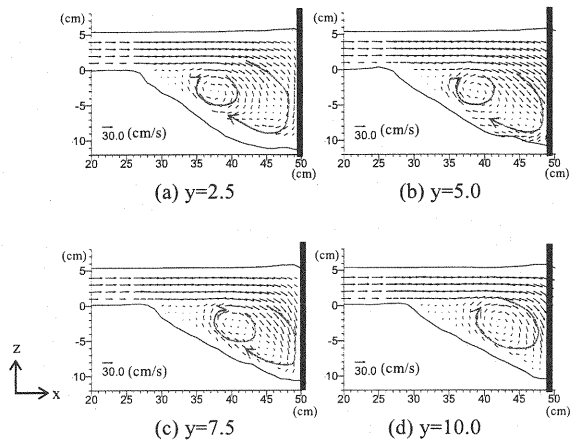

Fig. 13 Velocity vector (*u, w*) at the longitudinal sections (y=2.5, 5.0, 7.5, 10cm)

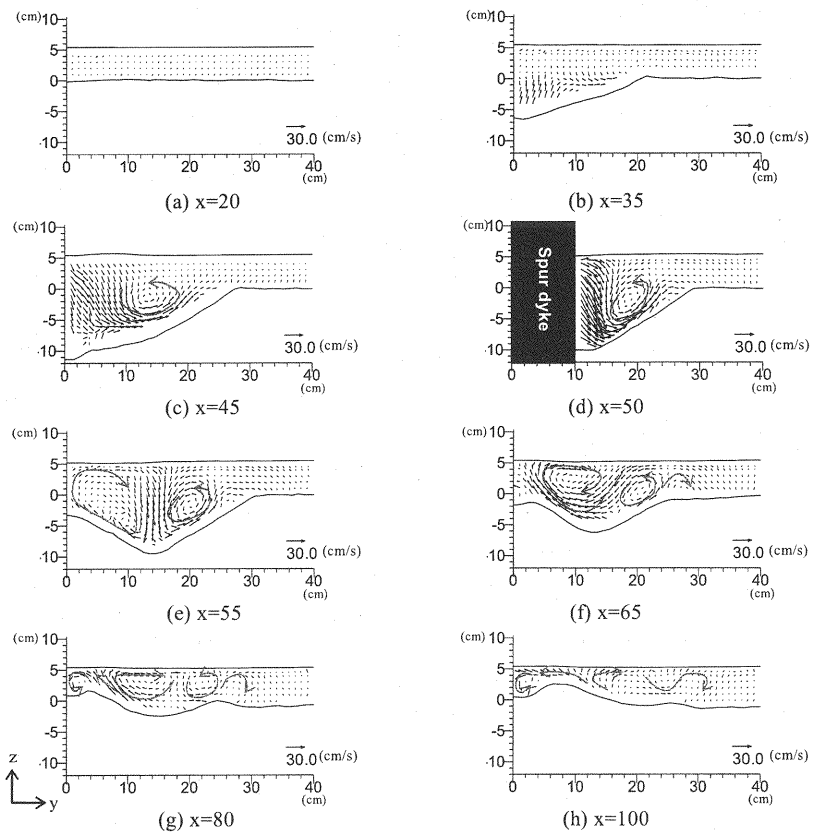

Fig. 14 Velocity vectors (*v, w*) at the cross section

The near bottom velocity 1.5cm above from the scoured bed level, which was measured by EMV, is shown in Figure 15. The measurement height was set due to the limitation of the instrument structure. The bottom velocity vector is useful for understanding the route of sediment transport. The bottom velocity vectors in the upstream region of the spur dyke and near its head region were directed toward the edge of scour hole, which was affected by the horse-shoe vortex. The velocity slowed locally due to flow convergence near the edge of the scour hole, and the directional change was also extreme near the edge. The distinctive point of this bottom-flow field is that the horse-shoe vortex and the wake vortex caused bottom flow-separation, which directed toward the sidewall behind the spur dyke region and main channel side, which started from the spur dyke section to downstream. The wake vortex was the driving force which could transport the sediment to behind the spur dyke, while the horse-shoe vortex was the driving force which could transport the sediment to main channel. The bottom-flow velocity was decreased somewhat in the scoured region and behind the spur dyke as compared to main channel region. In the downstream of spur dyke, the bottom flow velocity was accelerated as tongue shape. In the region enclosed in broken line in Fig. 15, the bottom flow was upturned due to the existence of horse-shoe vortex as shown in Fig. 14(e), (f), (g). Therefore, the horizontal velocity decreased to an extent as compared to the surrounding area. Thus, the bottom flow field around the spur-dyke was controlled by the vertical vortices.

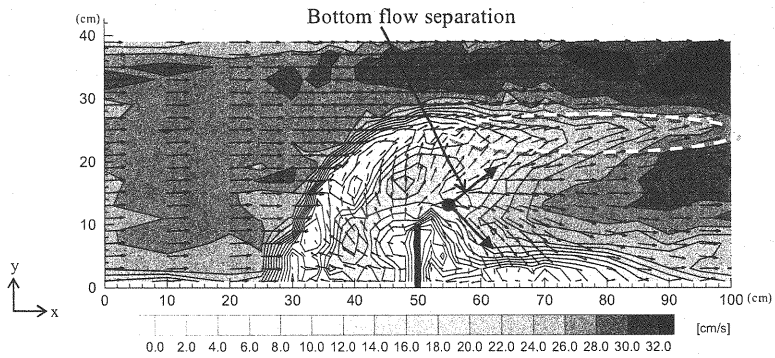

Fig. 15 Bottom velocity vectors and contour above 1.5cm from the bed

Grain-size variation around a spur dyke

The sediment heterogeneity had impact not only on the bed topography but also on the bed composition. The complex flow field around the spur dyke led to sediment sorting in both longitudinal and transverse directions. In the scour hole, bed materials in the surface layer turned into coarse sediments. The downstream side of the spur-dyke in main channel area also became significantly coarsened.

Figure 16 shows the results of the variation of the bed-surface composition. The colored circles and triangles indicate sampling points and their color show a change ratio of mean diameter (D_m/D_{m0}), which is the results of bed-surface mean diameter divided by initial one. The dark triangles showed the finer material points while the bright circles showed the coarser material points than initial condition. There were characteristic longitudinal fine sediment regions behind the spur dyke and near the center line of the flume. Thus we also measured its coordinates and grain-size distribution.

Figure 17 shows the initial and final data of grain-size distribution at the spur-dyke head. During the scour

process, relatively fine sediments were picked up and the bed gradually coarsened in all non-uniform sediment bed cases. In particular, M4 and M5 cases coarsened significantly and reduced the scour depth. There was a small quantity of sediment, whose size was smaller than 1.5mm, and which formed an armor coat layer with coarse sediment near the spur dyke head.

In all non-uniform sediment beds case, the outstanding coarsened region was formed in front of spur dyke and the longitudinal region from spur dyke head to the downstream. Furthermore, two longitudinal regions with fine sediment were formed on both sides of the longitudinal coarsening region. These sorted sediment regions resulted from the existence of two vortices and the interaction of local bed slope of the scour hole. The horse-shoe vortex and the wake vortex were located in a scour hole, and the vortices drove the sediment toward the edge of the scour hole. At that time, coarse sediment could not reach there because of the steep bed slope and its own weight. On the other hand fine sediment was picked up at the bottom, and reached near the scour-hole edge. Thus, the spatial coarse and fine sediment patterns formed due to vortices and to the local bed slope of the scour-hole during the scouring process. Furthermore, the fine sediment region near the flume center was located in the upward flow region and a relatively low tractive force region affected by the horse-shoe vortex is shown in Fig. 14 (d), (e), (f). The low tractive force region was also an important cause of formation of the fine sediment region near the flume center. In Case of M5, the fine sediment longitudinal region near the flume center did not exist. The M5 bed sediment was gap-graded consisting of two grain sizes (i.e. 2.38mm and 0.17mm), which were much different in grain size in these experiments. Since the scour hole of M5 case was small as compared to other cases, the tractive force did not decrease well. Therefore, the fine particles flushed away to downstream on the bed surface and did not form a longitudinal fine sediment region near the flume center.

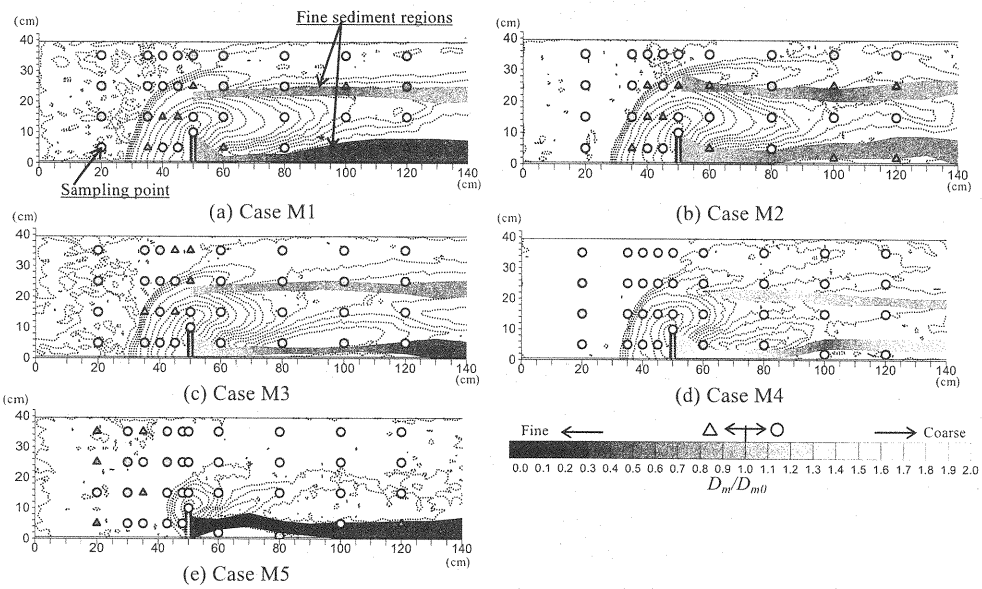

Fig. 16 Change ratio of mean diameter (D_m/D_{m0})

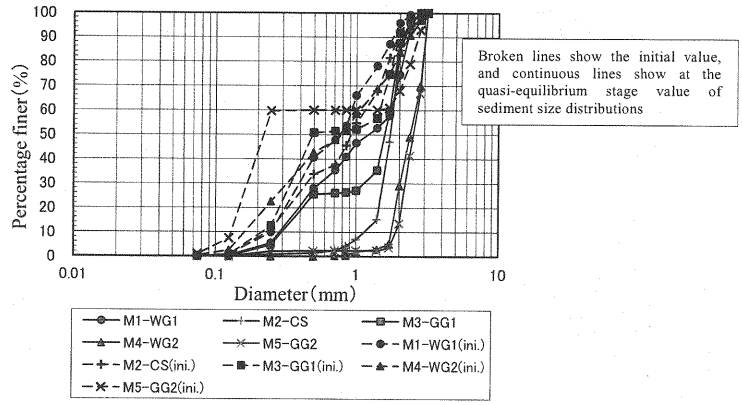

Fig. 17 Grain-size distributions at spur dyke head

Figure 18 shows an illustration of bed surface at the quasi-equilibrium stage in the Case M2 using color sand. The color of surface bed sediment in photograph was in good agreement with the measurement data as shown in Fig. 16 (b). We can see the usefulness of experiment by using color sediment to obtain an overview of the spatial variation of grain-size distribution in this photograph.

The longitudinal region of coarse black-sediment was wide, and the blue-sediment existed partially at the edge of predominant black-sediment region. We can see that the extreme variation of predominant grain-size at the boundary between the red and the black sediment regions. In addition, there were fine sediment regions at a somewhat inner region of scour-hole edge; it was difficult to find it non-colored sediment experiments. During the scouring process in front of the spur dyke, the more fine sediment was transported through an outer route compared to coarse sediment, due to the interaction among the horse-shoe vortex, steep bed slope and the differences of sediment weight.

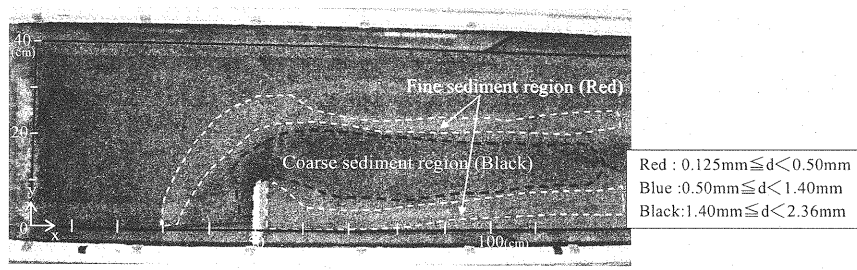

Fig. 18 Picture of final bed-surface for color sand experiment (Case 6)

Finally, Fig. 19 shows a schematic diagram of three-dimensional flow structure and transverse sediment sorting around a spur dyke, we mentioned above and clarified the matters in this study. The sketch indicates the difference between the surface flow and the bottom flow structure due to several vortex systems. Both the bed slope of the scour-hole and the complicated bottom flow field caused the significant coarse sediment region and fine sediment regions around the spur dyke.

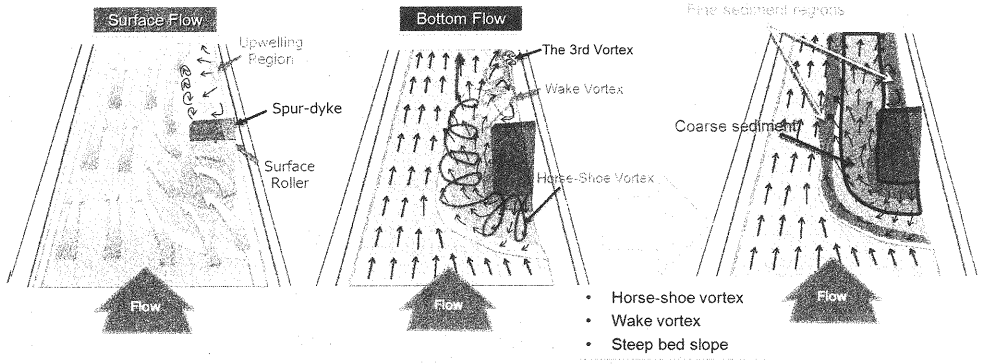

Fig. 19 Schematic diagram for 3D flow structure and sediment sorting

CONCLUSIONS

An experimental study on the change of channel bed configuration and grain size distribution around single impermeable spur-dyke under non-submerged condition was presented. A total of nine experiments were conducted, including relatively uniform/non-uniform sediment bed experiments. Findings show that installing a spur dyke not only enhanced diversities of channel morphologies, but also enhanced diversities of surface bed composition around the spur dyke. The main findings and conclusions of this study are summarized.

It was found that the sediment heterogeneity did not influence the typical scour-deposition morphological pattern but did influence on the detailed topographic features around the spur dyke structure. The mean grain size and the geometric standard deviation are two controlling parameters for a local scour around the spur dyke under specific flow conditions. The maximum scour depth and the scour area for relatively uniform sediment bed increased with decrease of the mean grain size in the clear water condition. In non-uniform sediment bed, the maximum scour depth was generally smaller compared to that in a uniform one with similar mean grain size. Furthermore, the maximum scour depth in the non-uniform sediment bed decreased with the increase of the geometric standard deviation if the mean grain size was kept constant.

The flow measurement data shows three-dimensional flow structure around the spur dyke on scoured bed at the quasi-equilibrium stage. The data clearly shows that the horse-shoe vortex and the wake vortex are dominant vortex for bed scouring and sediment sorting around spur dyke. The third vortex was measured near the sidewall, which was due to the upwelling flow which is part of wake vortex and bed shape of downstream of spur dyke. Furthermore, the measured data clarifies the horse-shoe vortex which consists of two vortices structure in the same direction of rotation near the sidewall in front of the spur dyke.

Bed material in the surface layer around the spur dyke significantly changed. Noticeable coarsened regions formed in front of the spur dyke, near the spur dyke toe, and longitudinal region from spur dyke toe to downstream. Besides, there generally existed two longitudinal belts consisting of relatively fine sediment compared with the surrounding area in the downstream of the spur dyke. The flow measurement data made it clear that the coarse sediment region and two fine sediment belts formed due to the interaction between vortex systems and the local bed slope of the scour hole. Furthermore, by means of movable bed experiment using color sediment, which was classified different sizes and colors, supplemented the information of spatial variation of bed surface composition. In

particular, it was revealed that there were fine sediment regions at the inner region of scour-hole edge, which were difficult to find by regular sampling data with non-colored sand. In movable bed experiments by means of non-colored sediment, it was difficult to measure the detailed spatial bed composition, because it was heavy work and required much time. In the present study, we have shown that using color sediment classified different size for movable experiments was effective in understanding the time/spatial variation of bed surface composition visually.

The experimental data, which was measured in a series of this study, is also useful in verifying the accuracy of the results of the numerical model. The grain-size distribution data is very few and especially useful in developing a numerical model which can predict grain-size variation around spur dykes. In further study, numerical models which accounting for the sediment sorting process are being developed.

ACKNOWLEDGEMENTS

This work was supported by Grant-in-Aid for Young Scientist (B), MEXT, JAPAN (PI: Dr. Hao Zhang, Grant No.22760369) and JSPS AA Science Platform Program (Coordinator: Dr. Hajime Nakagawa).

REFERENCES

1. Shimizu, Y., Koba, S., Kobayasi, T., Osada, K., Nakamura, Y. and Miyamae, T. : Study on restoration of riffle-pool structure in mountain river by using groin placement, Advances in River Engineering, Vol.10, JSCE, pp.411-416, 2004(in Japanese).
2. Fukudome, S., Fujita, S. and Fukuoka, S. : Design of low-water groin to recover environment of pool and the evaluation of environmental function, Annual Journal of Hydraulic Engineering, JSCE, Vol.54, JSCE, pp.1267-1272, 2010(in Japanese).
3. Michiue, M. and Hinokidani, O. : Calculation of 2-dimensional bed evolution around spur-dike, Annual Journal of Hydraulic Engineering, JSCE, Vol.36, JSCE, pp.61-66, 1992(in Japanese).
4. Muneta, N. and Shimizu, Y. : Numerical analysis model with spur-dike considering the vertical flow velocity distribution, Journal of the Japan Society of Civil Engineers, JSCE, No.497, 2-28, pp.31-39, 1994(in Japanese).
5. Zhang, H., Nakagawa, H., Kawaike, K., Baba, Y. : Experiment and simulation of turbulent flow in local scour around a spur dyke, International Journal of Sediment Research, Vol.24, No.1, pp.33-45, 2009.
6. Tominaga, A., Ijima, K. and Nakano, Y. : PIV analysis of flow structures around skewed spur dikes, Annual Journal of Hydraulic Engineering, JSCE, Vol.45, JSCE, pp.379-384, 2001(in Japanese).
7. Melville, B.W.: Pier and abutment scour: integrated approach, Journal of hydraulic Engineering, ASCE, Vol.23, pp.125-136, 1997.
8. Rahman, Md. M, and Muramoto, Y. : Prediction of maximum scour depth around submerged spur-dike-like structures, Annual Journal of hydraulic Engineering, JSCE, Vol.43, pp.623-628, 1999.
9. Nasrollahi, A., Ghodsian, M. and Neyshabouri, S.A.A.S. : Local scour at permeable spur dikes, Journal of Applied Sciences, 8(19), pp. 3398-3406, 2008.
10. Nagata, N., Hosoda, T., Nakato, T. and Muramoto, Y. : Three-dimensional numerical model for flow and bed deformation around river hydraulic structures, Journal of Hydraulic Engineering, ASCE, Vol.131, No.12, pp.1074-1087,2005.
11. Zhang, H., Nakagawa, H., Ishigaki, T., Muto, Y., and Baba Y. : Three-dimensional mathematical modeling of local scour, Journal of Applied Mechanics, Vol.8, pp.803-812, 2005.

12. Duan, J. G., He, L., Fu, X. and Wang Q. : Mean flow and turbulence around experimental spur dike, Advances in Water Resources, 32, pp.1717-1725, 2009.
13. Zhang, H., Nakagawa, H. and Mizutani, H. : Bed variation around spur dyke under non-uniform sediment transport, Proc. of 17th IAHR-APD Congress, Memory Stick, No.3a045, 2010.

APPENDIX – NOTATION

The following symbols are used in this paper:

a, b, c = dimensions of scour hole at designated section;

D_m = mean diameter of bed materials;

e_m, e_{m*} = dimensional and non-dimensional maximum scour depth;

g = gravity acceleration;

h = water depth;

L = length of the spur dyke;

U_* = friction velocity;

U_{*c} = critical friction velocity;

V_s = volume of the scour hole;

x, y, z = x- ,y- and z- coordinates;

θ = bed slope ; and

σ_g = geometric standard deviation of the sediment.

(Received Aug, 01, 2011 ; revised Apr, 02, 2012)